Model of secondary emission and its application on the charging of gold dust grains

I. Richterová,* J. Pavlů,† Z. Němeček,‡ and J. Šafránková§
Charles University, Faculty of Mathematics and Physics, V Holešovičkách 2, 18000 Prague, Czech Republic
(Received 21 August 2006; published 19 December 2006)

We present a combined experimental and simulation study of the charging of the spherical gold samples by an electron beam in a 0.15–10 keV range of beam energies. Experiments on grains with diameters of the order of 10^{-6} m show that the charge (or surface potential) of grains levitating in a guadrupole trap is a function of both grain diameter and beam energy. Monte Carlo simulations reveal that an increase of the grain potential with the beam energy for a fixed diameter or a surface potential decrease with the grain diameter for a given beam energy are connected with changes of the relative number of backscattered primary electrons. The results of simulations are in a good quantitative agreement with previously published as well as our fresh experimental data.

DOI: 10.1103/PhysRevB.74.235430 PACS number(s): 79.20.Hx, 94.05.Bf, 52.27.Lw

I. INTRODUCTION

Comets, planetary rings, exposed dusty surfaces, and the zodiacal dust cloud are all examples of environments where dusty plasma effects establish the size and spatial distributions of small grains. Simultaneously, dust often influences the composition, density, and temperature of the surrounding plasma. The dynamics of charged dust grains can be surprisingly complex and fundamentally different from the well-understood limits of gravitationally dominated motions of neutral particles or the adiabatic motion of electrons and ions in electromagnetic fields that dominate gravity.

While the study of dust–plasma interactions is not new, early progress in the field was slow and uneven. However, it received a major boost in the 1980s with the Voyager spacecraft observations of peculiar features in the Saturnian ring system ("radial spokes") which could not be explained by gravitation alone and led to the development of the gravito-electrodynamic theory of dust dynamics. This theory scored another major success more recently in providing the only possible explanation of collimated high-speed beams of fine dust grains from Jupiter observed by the Ulysses and Galileo spacecraft.[1] At present, several space missions (e.g., Cassini, Rosetta, Helios) provide (or will provide) direct observations of dust grains in the interplanetary space and in the Jovian and Saturnian systems to investigate their physical, chemical, and dynamical properties.[2–6]

Immersed in a plasma, the grain is charged due to its interaction with radiative and plasma environment. The grain charging depends on the physical and electrical properties of the grains, on the nature of their interaction with the surrounding radiation and plasma fields, and on the relative velocity. The most important contributions come from a flux of electrons and ions, from the UV-radiation induced photoemission, and from secondary emission of electrons. The surface potential of a dust grain is established by a balance between various charging currents and resulting potentials can range from about −10 kV in planetary magnetospheres[7] to some 10 V in an interplanetary space[8] depending on size, shape, material, and charging history of grains.

The calculation of the acquired net charge is generally a difficult task mainly due to the complicated processes involved and because the knowledge of the adequate dusts properties (such as photoemission efficiency, secondary electron emission yield, etc.) is required. These properties are usually deduced from experimental measurements made on bulk materials or planar surfaces. However, the highly curved surface of small dust grains may considerably change the corresponding physical properties, thus these properties may be a function of the grain size and its shape.

The theory and models are well developed for environments that vary from dense planetary atmospheres to diffuse environments such as interplanetary space. However, experimental investigations of individual dust grains in equilibrium are less common, perhaps due to the difficulty of these experiments. Laboratory simulations were started at the beginning of the 1990s. For example, Suszcynsky *et al.*[9] measured secondary electron yields from ammonia and methanol ices as a function of the electron beam energy in the 2- to 30-keV energy range and summarized that secondary electron yields are on the low end of the range for insulators ($\approx$1–25). Spann *et al.*[10] dealt with secondary electron emission of dust grains levitating in the Paul trap in a very narrow range of attainable charges. Švestka *et al.*[11] measured the secondary electron emission profile of dust grains using an electron beam up to 20 keV. They achieved a positive charge even at high electron energies and they attributed this effect to an emission from the opposite side of the grain. Similar experiments were prepared on submicron oil and micron nonspherical metal grains by Ziemann *et al.*[12] and Velyhan *et al.*,[13] respectively. However, they used lower beam energies and thus they did not observe the surface potential growth at high beam energies.

II. SECONDARY ELECTRON EMISSION

Primary electrons (PEs) impacting the sample surface interact with a bulk material and they lose their energy in many types of collisions and it often results in excitations of material electrons. Some of the excited electrons can then leave the surface. These electrons, so-called true secondary electrons (SEs), have typically energies of a few electronvolts. For large planar samples, the energetic dependence of the secondary emission yield, δ (defined as the mean number of

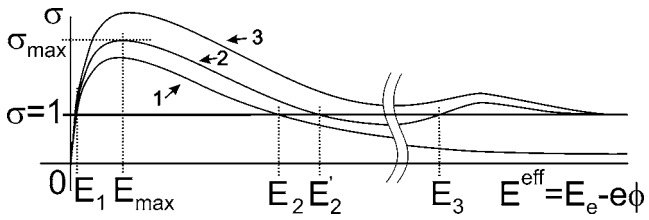

FIG. 1. Schematics of the total secondary emission yield as a function of the beam energy: (1) planar surface, (2) dust grain from the same material, and (3) dust grain from a material with a larger secondary emission yield.

SEs per one PE) can be described by the Sternglass universal curve.[14] This curve exhibits a maximum at a few tenths of kiloelectronvolts and decreases to zero at very high and low beam energies. Its parameters, the maximum yield δ_{max} and the corresponding energy E_{max} depend only on a sample material at a certain incident angle.

In collisions inside the target, PEs change their directions and thus they may be backscattered from the material before losing the whole energy. The backscattered yield η increases with the material density and the atomic number up to ≈ 0.5 for a normal incident angle. It grows only slowly with the beam energy above a few hundreds of electronvolts. Thus, the total secondary yield $\sigma = \delta + \eta$ and δ vary in a similar way with the beam energy.[15]

The energy dependence of a total secondary yield of dust grains does not fully follow the universal curve for large samples. It is enhanced due to a surface curvature that results in a variation of the incident angle along the grain surface because σ (and both constituents, δ as well as η) increases with an incident angle.[15] The secondary emission yield is enhanced by a factor of ≈ 1.3 for spherical grains. This enhancement does not change the profile of σ as a function of the primary energy in low- and mid-energy ranges. An energy dependence of σ and its variation with a sample shape is sketched in Fig. 1. The figure shows σ as a function of the primary energy for a planar surface (1) and for two dust grains (2) and (3). In a very low energy range, below an energy E_1, σ rises with the primary energy. Since $\sigma < 1$, all samples are charged negatively. This is a typical regime of the electron attachment. The rise of σ is terminated at E_{max}.

At higher energies ($E > E_{max}$), the PEs deposit their energy farther from the surface and σ decreases until it approaches unity (at E_2) for large samples. The sample is charged positively between E_1 and E_2, whereas a negative charge can be expected above E_2. On the other hand, depending on the grain size and material, the secondary emission yield can behave as it is shown by curves 2 or 3. The energy corresponding to $\sigma = 1$ can be shifted to higher energies (E_2') or even to infinity (curve 3) because the penetration depth of PEs increases with their energy and SEs leave the grain with a higher probability when the penetration depth of PEs becomes comparable with the grain size. This effect increases the value of σ and the decreasing trend of the profile reverses.

We would like to note that the rise of the total secondary emission yield at higher energies for small samples (curves 2 and 3) can be in principle caused by two factors: (1) by increase of the number of SEs due to emission from the "backside," this effect is well known as second-surface secondary electron emission from thin films, and/or (2) by increasing number of backscattered PEs. One of the aims of the present paper is to show that the second process is dominant for spherical samples.

At very high energies, the majority of PEs penetrate the grain without any energy loss and, thus, σ asymptotically approaches unity ($\delta \to 0$; $\eta \to 1$). Note that the grain behaving according to profile 2 will be charged negatively below E_1 and between E_2' and E_3, whereas grains following the profile 3 will be charged positively for all energies above E_1. The profiles like 3 were experimentally observed for glass samples[11,16] and profiles corresponding to curve 2 were reported by Richterová *et al.*[17] for grains from melamine-formaldehyde resin; all in micrometer range of sizes.

Theoretical treatments of secondary electron emission have been based on many different approaches. This emission has been described by the elementary theories of Salow,[18] Baroody,[19] and Bruining.[20] Kanaya and Kawakatsu[21] have modified these results by using a Lindhard power potential to describe SE emission from metals due to both primary and backscattered electrons (BEs), and Kanaya *et al.*[22] extended this approach to include insulators. A complex approach to the problem of electron-induced secondary electron emission can be found in Sternglass.[14] He found that the scattering of PEs inside the grain is principal for an explanation of the secondary emission. However, the validity of his already mentioned "universal curve" was limited to 4 E_{max}. Later, Draine and Salpeter[23] found a new approximation by fitting to experimental data and this approximation is valid to higher energies. A well-known and particularly useful theory for the emission of SEs from metals induced by energetic ions ($\geqslant$ a few megaelectronvolts) was proposed by Sternglass.[24] Suszcynsky *et al.*[9] modified this theory to predict the secondary electron yield from metals impacted by energetic (several kiloelectronvolts to about 200 keV) electrons. This modification accounts for the contribution of the BEs to the production of SEs based on knowledge of the BE energy distribution and the authors concluded that the modification is in reasonable agreement with the experimental data from gold targets in the 6–30-keV electron energy range.[25]

Simulation studies of secondary emission have been based mainly on a Monte Carlo electron trajectory simulation method which is a powerful tool for electron probe microanalysis, electron spectroscopy, and microscopy[26–28] where the target influenced by the electron beam is studied. These papers focus on various aspects of these phenomena (e.g., insulating target and internal fields,[29,30] insulating target and high and well-focused electron beams, respectively,[31–33] or electron-induced electron emission from inorganic insulators[34]).

A series of the papers by Ding *et al.*[35–37] precises a Monte Carlo simulation model of electron interactions with solids that includes cascade SE production. The model is based on the use of Mott's elastic scattering cross sections[38] and Penn's dielectric function approach[39] to electron inelastic scattering. The absolute primary energy dependence of the secondary yield and the energy distribution of SEs have been

obtained[37] and the authors noted a good agreement between the model and experimental data measured for clean Cu samples[40] in ultrahigh vacuum. Systematic investigations of SE generation and emission for 19 metals were published in Ding *et al.*[35] The calculated secondary yield curve for a primary beam energy ranging from 100 eV to 2 keV was found to correspond with experimental universal curve. The calculations indicated that the characteristic energy loss of PEs may result in a corresponding feature in the energy distribution of SEs.

Ding *et al.*[36] have used the model approach to calculate the full energy distribution of BEs from the elastic peak down to the true-secondary-electron peak. They compare calculated spectra and experimental data measured with a cylindrical mirror analyzer for primary beam energies ranging from 0.5 to 10 keV at normal incidence for the pure Au, Ag, and Cu polycrystalline samples. A reasonable agreement was reached for the backscattering background at primary energies in the kiloelectronvolt region.

As we noted above, the majority of models were applied on the planar metal or insulating targets but less papers deal with spherical samples. Theoretical considerations of the secondary emission from submicrometer oil drops of spherical shapes were done by Ziemann *et al.*[12] They achieved a good matching with their experiment up to 250 eV of the primary energy. Chow *et al.*[41] developed a model of secondary emission from spherical bodies. The authors assume that the primary electron current density is conserved inside the grain, PEs move straight inside the grain, the production rate of SEs is proportional to the energy loss of PEs, and the escaping probability of SEs decreases exponentially with a distance to the surface. They added the Whiddington law for energy losses along their path in the grain and computed the yield of secondary emission (similarly as in Dionne[42]). Their computation, in fact, assumes that the PEs move along straight lines inside the grain but the SEs can proceed toward the surface in any direction. Since their model did not reproduce the Švestka *et al.*[11] experimental data, Chow *et al.*[43] published an improved model. The new model provided the curve of the yield of secondary emission with several maxima. Varying the constants of the model, the authors were able to fit the data but they should use different sets of constants for low- and high-energy regions.

Richterová *et al.*[44] developed a simple Monte Carlo model of secondary emission from spherical dust grains. Although the model provides a typical secondary yield curve and can roughly describe observed energetic dependences of a dust grain equilibrium charge, it has numerous nonmeasurable parameters. Moreover, neither backscatter yield nor dependence on a sample material match the experimental data very well. Thus, we have prepared a new model based on more realistic assumptions and discuss the results in view of present knowledge of the electron–solid interaction as well as our fresh experimental data.

III. PREVIOUS MODEL FOR THE SPHERICAL GRAIN CHARGING

In Richterová *et al.*,[44] we have used the original Sternglass[14] approach and performed a computer Monte Carlo model of secondary emission from small bodies. The model follows individual trajectories of PEs inside the grain and, based on simple assumptions consistent with the Sternglass theory, calculates a probability of escaping of the excited electrons. The basic assumptions of the model were the following:

(1) The grain is spherical and consists of a continuous and homogeneous matter characterized by a few material constants and no detailed real atomic or electronic structures are included. This assumption means that grains are large enough. The model cannot be valid for small atomical/molecular clusters often present in the space. On the other hand, using the grain radius approaching infinity, the model can be used as a rough approximation of planar samples.

(2) PEs penetrate into a grain and undergo collisions with grain atoms and move along a straight line between collisions. The PE direction is altered after each collision according to a simple distribution like a cosine law (independently on the PE energy). The length of the primary electron path between two consecutive collisions, λ, is proportional to its current energy, E: $\lambda=\lambda_0\cdot(E/\Delta E)$, where λ_0 and ΔE are the material-dependent parameters of the model.

(3) One material electron is excited during each collision and then it behaves independently on the PE.

(4) A probability, $P=A\cdot\exp(-x/\Lambda)$, that the excited SE reaches a grain surface decreases exponentially with a distance from the surface x. Constant A normalizes the integral probability to be equal to $1/2$ when the electron is on the surface of a grain with the infinite diameter. The mean free diffusion path of SEs, Λ, is expected to be of the order of a lattice constant for metals and much longer for insulators.[14] The resulting probability of the escape of excited electron is then calculated by integration of the probability around the whole grain surface.

(5) For an equilibrium grain potential modeling, the SE energy spectrum must be employed. In accord with the third assumption, we suppose that this spectrum does not vary with the beam energy. A random energy in accordance with a chosen distribution is generated for each SE and it escapes from the grain when this energy is larger than the actual grain potential.

Although the model provides relevant δ curve, a number of BEs remains independent on material and exceeded significantly experimental values as a consequence of the second assumption. Moreover, the model includes several free parameters $(\Delta E, \lambda_0, \Lambda)$ which can be determined by a fit of model results to the experimental data only. Nevertheless, the grain potential growth at the high-energy beam range was predicted. It was shown that this growth is caused by the η enhancement and not by the δ increase as suggested by Chow *et al.*[43] and Švestka *et al.*[11]

IV. NEW VERSION OF THE MODEL

The above discussion has shown that the scattering of PEs inside the grain is a principal factor for the grain charging due to secondary emission because it determines the number of BEs and coefficient η. For this reason, we have applied energy- and material-dependent cross sections often used in

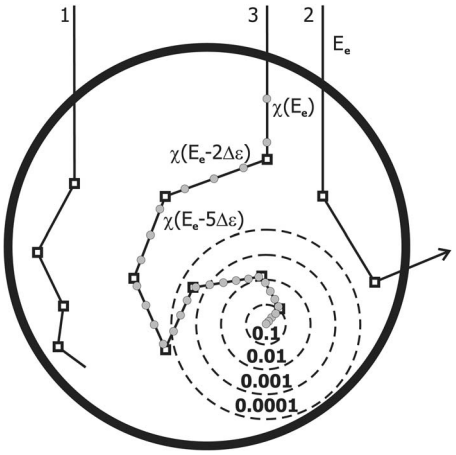

FIG. 2. A 2D demonstration of model assumptions.

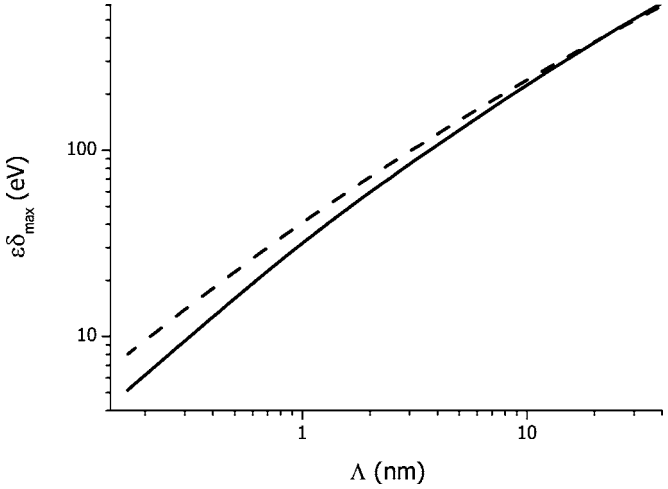

FIG. 3. $\epsilon\delta_{\max}$ product as a function of the mean free diffusion path (see text for the full description)

modeling of the beam–solid interaction for an electron microscopy[40] into our new model. This application requires modification of aforementioned assumptions in the following way:

(1) Assumptions of (1), (4), and (5)—without modifications.

(2) For description of PE trajectories inside the matter, a single scattering model according to Hovington *et al.*[45] is used:

• A PE moves along straight lines between collisions. Since almost all non-negligible deflections are caused by elastic electron-atom collisions above several hundreds electronvolts,[46] Mott radial elastic cross sections,[38] namely values computed by Czyżewski *et al.*,[47] are employed. Since their computations were made for several energies between 20 eV and 30 keV only, we have used a cubic spline interpolation for intermediate values. Advantages of this approach (instead of any approximative function usually used[40]) are a better accuracy as well as a shorter computation time.

• All possible energy losses are averaged and thus each PE loses the energy continuously along its path according to the modified Bethe stopping power equation. This modified equation can be written as

$$\frac{dE}{ds} \sim \rho \frac{Z}{AE} \ln\left(\frac{1.166E}{J}\right),$$

where ρ is the sample mass density, Z and A are the atomic and neutron numbers, respectively, J is close to the mean ionization potential, ds is the path element, and E is the actual electron energy.[45]

(3) Whole deposited energy is converted to electron excitations. The number of excited electrons is related to the energy spent by the mean excitation energy ε. Excited material electrons behave independently on the collision type and/or on the PE energy or direction.

The principles of the model are illustrated in Fig. 2. Note that this is only a two-dimensional (2D) sketch but the model is 3D. PEs are scattered in elastic collisions (marked by squares) according to Mott's elastic scattering cross sections and their actual energy. Some of them are stopped in the grain (trajectory 1), while the others leave it (trajectory 2). Continuous energy losing given by the Bethe stopping power formula is realized by small discrete energy losses, $\Delta\varepsilon$, along the path (marked by circles) until the whole energy of the PE is spent. Material electrons are excited at these coordinates with a probability $\Delta\varepsilon/\varepsilon$ and the probability that they reach the surface decreases exponentially with the distance (demonstrated only for the last energy loss).

Only three free parameters—ε, Λ, and a SE spectrum—remain in our model and their influence on the model results will be examined in several following figures. However, we should note prior to the analysis that the mean ionization potential ε and the relative number of true secondary electrons δ are strongly coupled quantities. An increase of ε leads to a smaller number of ionizations along the PE path and thus to a decrease of δ. For this reason, their product $(\varepsilon\delta_{\max})$ is plotted in the following figures. Taking into account that the experimental value of $\delta_{\max}$ is close to unity for Au planar samples,[48] Fig. 3 shows that ε and Λ cannot be chosen independently in fitting to experimental data. On the other hand, one can see that the spherical grain exhibits several times larger $\delta_{\max}$ than planar samples in any reasonable range of Λ. In order to further decrease the ranges of ε and Λ for a future fitting of model results to experiments, Fig. 4 shows how the product $\varepsilon\delta_{\max}$ changes with a position of the maximum of secondary emission yield $E_{\max}$. The dependences were obtained varying Λ as those in Fig. 3 and a linear relation was found.

V. EVALUATION OF THE MODEL

The model is developed for a study of the charging of dust grains. Since there is a lack of such data, we are comparing the model results with experiments on planar surfaces in this chapter. As we have shown above, the energy spectrum of BEs is of principal importance. Figure 5 shows such spectra for a planar Au sample bombarded by the electron beam of several energies. One can note that the spectra match experiments and/or previous models (compare with Fig. 1 in Ding *et al.*[36]).

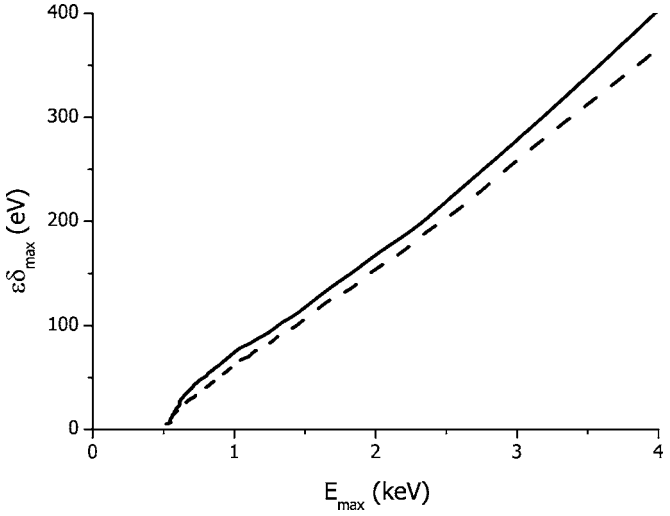

FIG. 4. $\epsilon\delta_{\max}$ product as a function of the energy corresponding to the maximum of secondary emission yield.

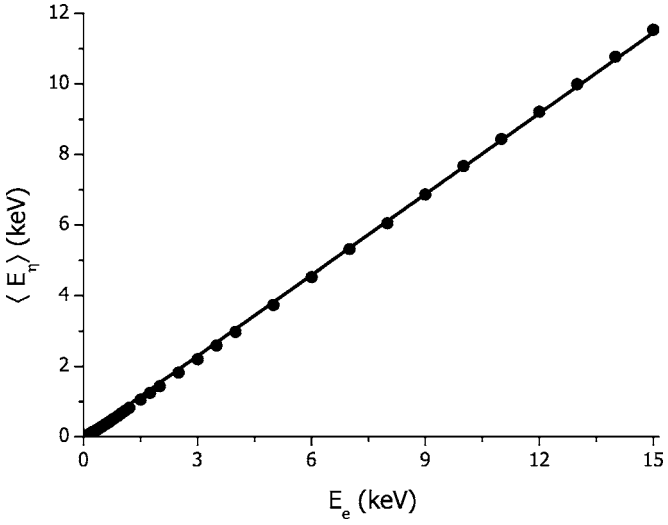

FIG. 6. Mean energy of backscattered electrons as a function of the beam energy.

BEs do not deposit their charge inside the target and thus, they do not contribute to the charging of the dust grains if their energy is high enough to overcome the grain potential. Figure 6 shows that the mean energy of BEs rises approximately linearly with the beam energy and the slope of a fit is ≈ 0.76. In other words, since η is roughly constant above 1 keV as we will show later, BEs carry out of the grain a constant fraction of the initial beam energy.

Summing all energy losses of PEs along the coordinate parallel with the beam axis, the distribution of beam energy losses in the sample can be obtained. Such data for several energies are plotted in Fig. 7 as a function of the depth beneath the sample surface x. A logarithmic scale has been chosen in order to show all curves in one figure. The position of the maximum of the energy losses increases with the beam energy E_e. The plot of this depth ($x_{\max}$) as a function of E_e in Fig. 8 reveals that this function can be approximated as $x_{\max}=k\cdot E^n$ where $n=3/2$ and $k=1$ in plot units. This function is not interesting for bulk targets influenced with primary energies above 1 keV because $x_{\max}$ is so large that the escaping probability of SEs from this depth is nearly zero. On the other hand, it can be important for dust grains (or thin films) when the grain size becomes comparable with $x_{\max}$.

Different assumptions and simplifications lead to different values of the exponent in the above equation. Its value ranges from 1 to 2 (if the scattering is neglected).[40] Sternglass[14] made a precise study of a secondary emission process that led to profiles of energy losses very similar to those in Fig. 7. On the contrary to many other authors, he supposed that the beam scattering is fundamental for the beam–solid interaction. He assumed that a non-negligible part of the PEs undergoes collisions which lead to a serious energy losses due to production of UV photons or Auger electrons. The re-absorbtion of these particles arises in a narrow peak of the distribution of beam energy losses close to the surface, and a peak position varies as a square root of an initial beam energy. Although the value of this exponent

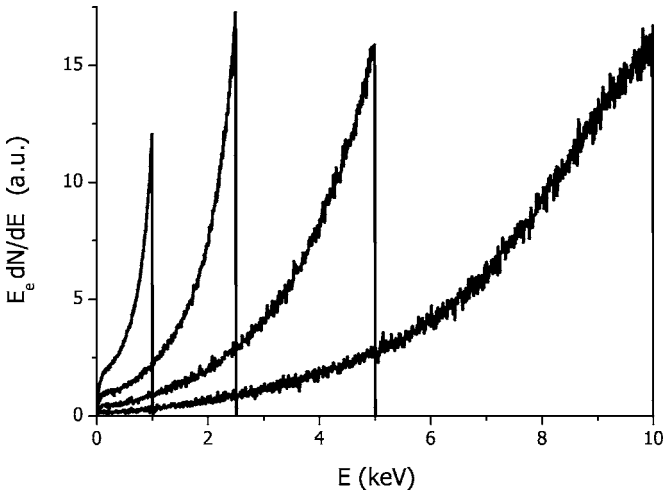

FIG. 5. Calculated spectra of backscattered electrons for several beam energies.

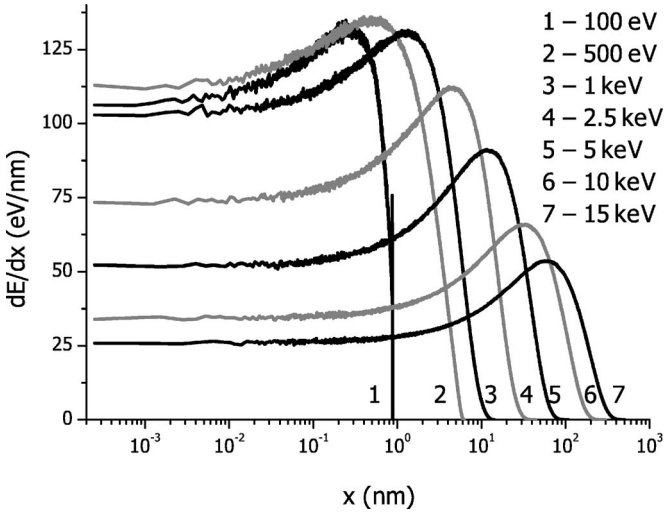

FIG. 7. Energy deposited per unit depth as a function of the distance from the planar sample surface for several beam energies.

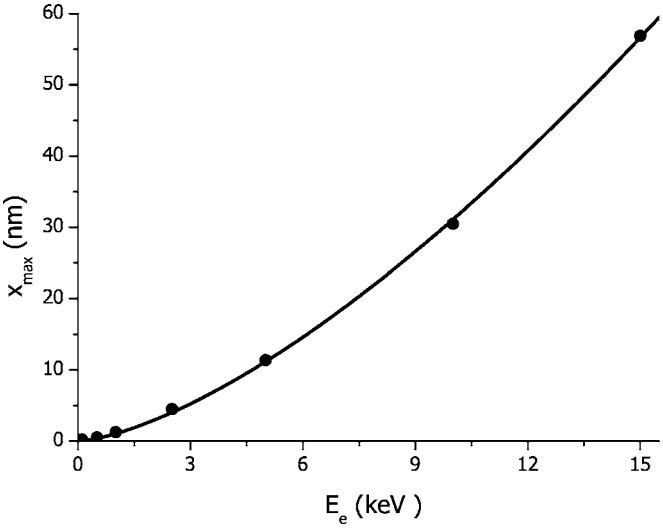

FIG. 8. Location of the maximum of energy deposition as a function of the beam energy.

would be very important for a decision among different models of the scattering inside the material, it cannot be measured and thus, we are leaving this point without comments.

VI. COMPARISON OF THE MODEL WITH EXPERIMENTAL DATA AND DISCUSSION

We have shown that our model describes details of secondary emission with a reasonable accuracy and thus, we can discuss effects connected with a finite size of dust grains. Figure 9 shows the secondary emission yield δ as a function of the beam energy for several diameters of spherical Au targets. The computed yield for a planar sample and "universal" curve[23] are given for the sake of reference. Taken into account the spread of the data used for a determination of this universal curve, we can consider the model results as

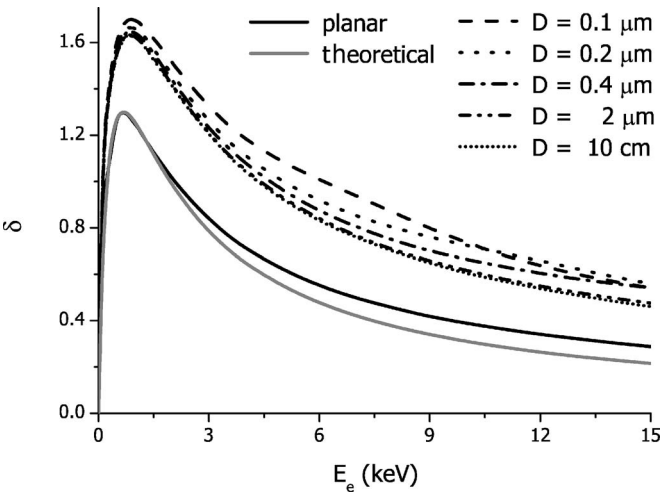

FIG. 9. Calculated energetic profiles of true secondary emission yield for the planar gold sample and several diameters of spherical samples. The universal curve of Draine and Salpeter[23] is given for reference.

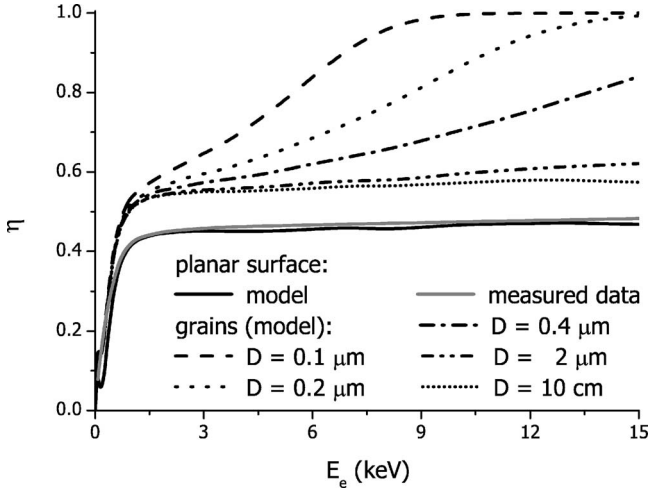

FIG. 10. Calculated energetic profiles of backscattered yield for planar gold sample and several diameters of spherical samples. Experimental data measured on a planar surface from Bronstein and Fraiman[15] are shown for comparison.

satisfactory. Moreover, the yield of true secondary electrons has only a small effect on resulting grain charge, as we will show later. On the other hand, our model neglects the production of x rays. A part of the produced photons leaves the grain and, thus, one can expect that δ provided by the model can be larger than experimental values especially at higher beam energies.

The principal rise of the yield δ is connected with the curvature of the grain surface but we did not find any difference in yields computed for 10 cm and 2 μm grains. A notable increase of the yield can be found for grain diameters below ≈ 1 μm. This increase is more pronounced at higher energies and can be probably attributed to the fact that a larger fraction of the primary energy is deposited near the surface as it follows from Fig. 7. Such effect would lead to a distinct maximum on secondary emission yield profile for thin films but, for spherical grains, it results only in a relatively small enhancement of δ for particular diameter in a certain range of energies (e.g., around 7 keV for the 0.1 μm grain).

The changes of the amount of true secondary electrons due to a finite size of the grain are of the order of several percent. On the other hand, the increase of the number of BEs is more distinct as it can be seen in Fig. 10. The calculated yield η for a planar sample matches exactly the experimental values taken from Bronstein and Fraiman.[15] The spherical surface of the grain leads to an increase of η from ≈ 0.45 to 0.55 in the high-energy range. The effects of finite grain dimensions start from a diameter of about 2 μm and η increases to nearly unity for smaller grains and high energies of PEs. Since the total secondary electron yield is a sum of δ and η, we can conclude that the rise of η represents a principal contribution to the increasing amount of electrons leaving small dust grains.

A comparison of analyzed effects with experimental data obtained on small grains is difficult because such observations are generally missing. The measurements on glass samples made by Švestka *et al.*[11] cannot be used for a quan-

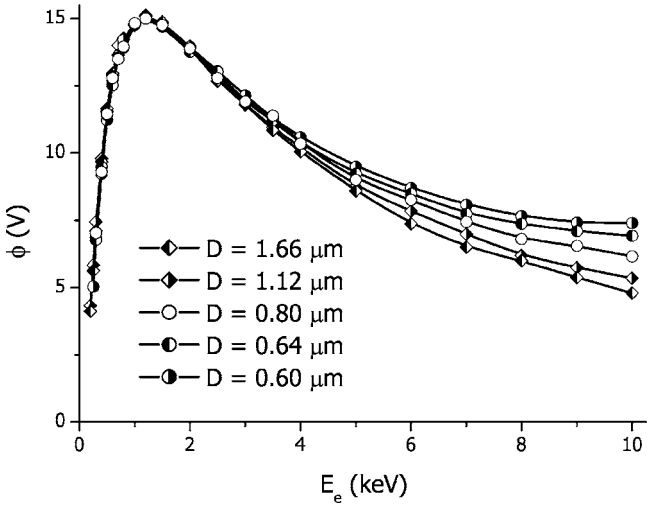

FIG. 11. Surface potential as a function of the beam energy as measured on several gold grains of different diameters.

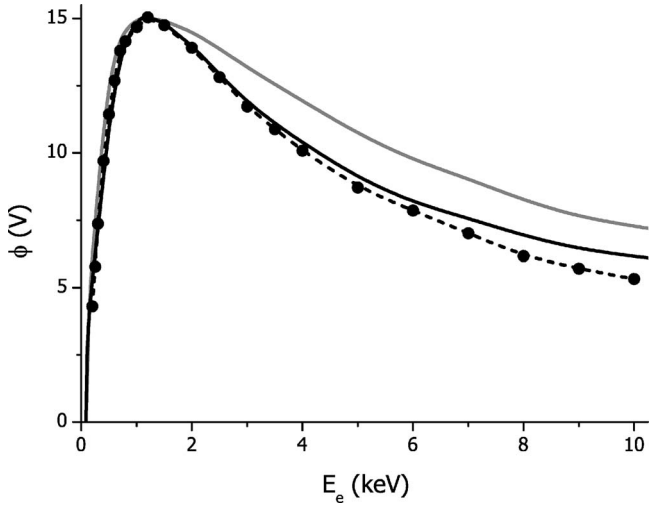

FIG. 12. Comparison of measured and calculated grain potentials. Grey (upper) curve uses Maxwell distribution, black (lower) curve uses Draine and Salpeter[23] distribution, and the experimental points are connected with the dashed line.

titative analysis because the composition of glass used for measurements is unknown. For this reason, we have carried out a series of measurements of charging characteristics on gold spherical grains. Details of the experiment are described elsewhere.[49–51] The experiment provides the grain potential as a function of the electron beam energy. Our experimental setup allows us to measure surface potentials of gold grains larger than ≈ 0.5 μm under primary energies in a range of 0.15–10 keV. Model calculations presented in Figs. 9 and 10 show that effects of the grain dimension would be small but observable. The measurements for five grains of different diameters are shown in Fig. 11. The profile roughly resembles an energetic dependence of the secondary emission yield (compare with Fig. 9) but the differences among grain potentials at larger energies (above ≈ 5 keV) cannot be explained this way. Nevertheless, Fig. 10 suggests that changes of the backscattered yield are responsible for a rise of the potential with a decreasing grain diameter.

A quantitative analysis of experimental data requires an assumption on the energy distribution of true secondary electrons (note that the spectrum of BEs is provided by the model). Although an energy spectrum of SEs is generally expected to be Maxwellian-like, Velyhan *et al.*[13] showed that the Draine-Salpeter distribution[23] seems to be more suitable for metallic grains.

Other two-model parameters (mean free diffusion path of SEs, Λ, and characteristic energy loss, ε) can be determined directly by a comparison of measured profiles with the results of computation in several steps:

- Since the maximum of $\phi(E_e)$ should correspond to the maximum of $\delta^*(E_e)$, the profiles of $\delta^*(E_e)$ were computed for different Λ. Among them, that peaking for the same E_e as measured profile $\phi(E_e)$ has been chosen ($\Lambda = 1.25$ nm).
- Knowledge of Λ allows us to find a value of the product $\varepsilon\delta_{\max}$ in Fig. 4 ($\varepsilon\delta_{\max} = 40.3$ eV).
- Since $\delta_{\max} = 1.3$ for a planar Au sample,[48] $\varepsilon = 31$ eV.

As a last step, the model was running with both aforementioned energy distributions of SEs and those potential profiles exhibiting the same values of maxima as measured data are plotted in Fig. 12.

The computations confirm the conclusion of Velyhan *et al.*[13] that the Draine-Salpeter distribution is more appropriate for metals because the Maxwellian distribution provides a much broader peak of the ϕ profile. On the other hand, there is no physical reason preferring a particular shape of distribution of SEs and thus, we cannot speculate if the difference between model and experimental results is connected with this distribution or with other simplifications used in the model. The distribution of SEs from dust grains can be measured in our experimental setup[52] and thus we plan to study it in detail.

VII. CONCLUSION

Our numerical and experimental investigations of the charging of dust grains illuminated by the electron beam have shown that a present version of the developed model describes very well basic features of measured profiles of the secondary electron yields for planar targets as well as the surface potential of small spherical grains. Consequently, we can conclude that the model includes principal processes leading to the emission of secondary electrons.

A further development of the model would include the x-ray production inside grains and excitation of secondary electrons this way. We think that these processes are responsible for an excess of the secondary emission yield in our calculations. A detailed experimental investigation of the energy distribution of true secondary electrons is necessary for a precise prediction of the grain potential.

ACKNOWLEDGMENTS

This work is a part of the research plan MSM 0021620834 that is financed by the Ministry of Education of the Czech Republic.

*Electronic address: ivana.richterova@mff.cuni.cz
†Electronic address: jiri.pavlu@mff.cuni.cz
‡Electronic address: zdenek.nemecek@mff.cuni.cz
§Electronic address: jana.safrankova@mff.cuni.cz

[1] M. Horanyi, Annu. Rev. Astron. Astrophys. **34**, 383 (1996).
[2] R. Srama, T. J. Ahrens, N. Altobelli, S. Auer, J. G. Bradley, M. Burton, V. V. Dikarev, T. Economou, H. Fechtig, M. Görlich *et al.*, Space Sci. Rev. **114**, 465 (2004).
[3] M. Horányi, T. W. Hartquist, O. Havnes, D. A. Mendis, and G. E. Morfill, Rev. Geophys. **42**, RG4002 (2004).
[4] N. Altobelli, E. Grün, and M. Landgraf, Astron. Astrophys. **448**, 243 (2006).
[5] F. Spahn, K.-U. Thiessenhusen, J. E. Colwell, R. Srama, and E. Grün, J. Geophys. Res. **104**, 24111 (1999).
[6] F. Spahn, J. Schmidt, N. Albers, M. Hörning, M. Makuch, M. Seiß, S. Kempf, R. Srama, V. Dikarev, S. Helfert *et al.*, Science **311**, 1416 (2006).
[7] H. Kimura and I. Mann, Astrophys. J. **499**, 454 (1998).
[8] E. C. Whipple, Rep. Prog. Phys. **44**, 1197 (1981).
[9] D. M. Suszcynsky, J. E. Borovsky, and C. K. Goertz, J. Geophys. Res., [Solid Earth] **97**, 2611 (1992).
[10] J. Spann, M. Abbas, C. Venturini, and R. Comfort, Phys. Scr., T **T89**, 149 (2001).
[11] J. Švestka, I. Čermák, and E. Grün, Adv. Space Res. **13**, 199 (1993).
[12] P. Ziemann, P. Liu, D. Kittelson, and P. McMurry, J. Phys. Chem. **99**, 5126 (1995).
[13] A. Velyhan, Z. Němeček, and J. Šafránková, in *WDS'01 Proceedings of Contributed Papers: Part II—Physics of Plasmas and Ionized Media*, edited by J. Šafránková (Matfyzpress, Prague, 2001), pp. 267–272.
[14] E. J. Sternglass, Master's thesis, Cornell University (1951).
[15] I. M. Bronstein and B. S. Fraiman, *Secondary Electron Emission* (Nauka, Moskva, 1969), in Russian.
[16] Z. Němeček, J. Pavlů, J. Šafránková, I. Richterová, and I. Čermák, in *Dusty Plasmas in the New Millennium*, edited by R. Bharuthram, M. Hellberg, P. Shukla, and F. Verheest, AIP Conf. Proc. No. 649 (AIP, Melville, New York, 2002), pp. 378–381.
[17] I. Richterová, J. Pavlů, Z. Němeček, J. Šafránková, and M. Jeřáb, in *New Vistas in Physics of Dusty Plasmas*, edited by L. Boufendi, M. Mikikian, and P. K. Shukla, AIP Conf. Proc. No. 799 (AIP, Melville, New York, 2005), pp. 395–398.
[18] H. Salow, Phys. Z. **41**, 434 (1940).
[19] E. M. Baroody, Phys. Rev. **78**, 780 (1950).
[20] H. Bruining, *Physics and Applications of Secondary Emission* (Pergamon, London, 1954).
[21] K. Kanaya and H. Kawakatsu, J. Phys. D **5**, 1727 (1972).
[22] K. Kanaya, S. Ono, and F. Ishigaki, J. Phys. D **11**, 2425 (1978).
[23] B. Draine and E. Salpeter, Astrophys. J. **231**, 77 (1979).
[24] E. Sternglass, Scientific Paper 6-94410-2-P9, Westinghouse Research Laboratories, Pittsburgh 35 (1957).
[25] D. M. Suszcynsky and J. E. Borovsky, Phys. Rev. A **45**, 6424 (1992).
[26] D. C. Joy, J. Microsc. **147**, 51 (1987).
[27] R. Shimizu and Z.-J. Ding, Rep. Prog. Phys. **55**, 487 (1992).
[28] A. Dubus, J.-C. Dehaes, J.-P. Ganachaud, A. Hafni, and M. Cailler, Phys. Rev. B **47**, 11056 (1993).
[29] J. P. Ganachaud, C. Attard, and R. Renoud, Phys. Status Solidi B **199**, 175 (1997).
[30] C. Attard and J. P. Ganachaud, Phys. Status Solidi B **199**, 455 (1997).
[31] R. Renoud, C. Attard, J.-P. Ganachaud, S. Bartholome, and A. Dubus, J. Phys.: Condens. Matter **10**, 5821 (1998).
[32] R. Renoud, F. Mady, and J.-P. Ganachaud, J. Phys.: Condens. Matter **14**, 231 (2002).
[33] R. Renoud, F. Mady, C. Attard, J. Bigarré, and J.-P. Ganachaud, Phys. Status Solidi A **201**, 2119 (2004).
[34] J. Cazaux, Nucl. Instrum. Methods Phys. Res. B **244**, 307 (2006).
[35] Z. J. Ding, X. D. Tang, and R. Shimizu, J. Appl. Phys. **89**, 718 (2001).
[36] Z. J. Ding, H. M. Li, K. Goto, Y. Z. Jiang, and R. Shimizu, J. Appl. Phys. **96**, 4598 (2004).
[37] Z. J. Ding, H. M. Li, X. D. Tang, and R. Shimizu, Appl. Phys. A: Mater. Sci. Process. **78**, 585 (2004).
[38] N. F. Mott and H. S. W. Massey, *Theory of Atomic Collisions* (Oxford University Press, New York, 1965).
[39] D. R. Penn, Phys. Rev. B **35**, 482 (1987).
[40] D. Joy, *Monte Carlo Modeling for Electron Microscopy and Microanalysis* (Oxford University Press, New York, 1995).
[41] V. Chow, D. Mendis, and M. Rosenberg, J. Geophys. Res., [Space Phys.] **98**, 19065 (1993).
[42] G. F. Dionne, J. Appl. Phys. **46**, 3347 (1975).
[43] V. Chow, D. Mendis, and M. Rosenberg, IEEE Trans. Plasma Sci. **22**, 179 (1994).
[44] I. Richterová, Z. Němeček, J. Šafránková, and J. Pavlů, IEEE Trans. Plasma Sci. **32**, 617 (2004).
[45] P. Hovington, D. Drouin, and R. Gauvin, Scanning **19**, 1 (1997).
[46] R. F. Egerton, *Electron Energy-loss Spectroscopy in the Electron Microscope* (Plenum, New York, 1996).
[47] Z. Czyżewski, D. O'Neill MacCallum, A. Romig, and D. C. Joy, J. Appl. Phys. **68**, 3066 (1990).
[48] H. Seiler, J. Appl. Phys. **54**, R1 (1983).
[49] I. Čermák, E. Grün, and J. Švestka, Adv. Space Res. **15**, 59 (1995).
[50] P. Žilavý, Z. Sternovský, I. Čermák, Z. Němeček, and J. Šafránková, Vacuum **50**, 139 (1998).
[51] J. Pavlů, A. Velyhan, I. Richterová, Z. Němeček, J. Šafránková, I. Čermák, and P. Žilavý, IEEE Trans. Plasma Sci. **32**, 704 (2004).
[52] P. Žilavý, I. Richterová, Z. Němeček, J. Šafránková, and J. Pavlů, Czech. J. Phys. **55**, 1283 (2005).